Neuroscience 164 (2009) 1701–1711

ESTIMATING INTRACELLULAR Ca^{2+} CONCENTRATIONS AND BUFFERING IN A DENDRITIC INHIBITORY HIPPOCAMPAL INTERNEURON

C. W. LIAO AND C. C. LIEN*

Institute of Neuroscience and Brain Research Center, National Yang-Ming University, 155, Section 2, Li-Nong Street, Taipei 112, Taiwan, Republic of China

Abstract—Calcium is known to regulate several phenomena like neuronal excitability and plasticity. Interestingly, the spatiotemporal profile of dendritic calcium depends on several processes, specific to each neuronal type. In this study, we investigated Ca^{2+} buffering and action potential (AP)-evoked Ca^{2+} signaling in the dendrites of anatomically identified oriens lacunosum-moleculare (O-LM) cells, a major type of dendrite-targeting interneurons in the hippocampal CA1 region, using a combination of whole-cell patch-clamp recording and fast Ca^{2+} imaging in acute rat brain slices. Cells were loaded with fluorescent Ca^{2+} indicators fura-2 or Oregon Green BAPTA-1 (OGB-1) via patch-clamping electrode, and the effect of fura-2 on AP-evoked dendritic Ca^{2+} transients was determined by ratiometric Ca^{2+} imaging. To estimate intracellular Ca^{2+} concentrations ($[Ca^{2+}]_i$) and endogenous Ca^{2+}-binding ratio (κ_s) in the proximal dendrite, fluorescence signals were converted into $[Ca^{2+}]_i$ using the ratioing method and were analyzed on the basis of the "single compartment model." Resting $[Ca^{2+}]_i$ was 22±5 nM and the build-up of $[Ca^{2+}]_i$ during a single AP was up to 656±226 nM. Analysis of Ca^{2+} transients revealed that O-LM cells have a relatively low endogenous Ca^{2+}-binding ratio (κ_s): the κ_s was 20±8 estimated during fura-2 loading and 27 estimated under steady-state fura-2 concentrations, respectively. To further examine the spatial profile of dendritic Ca^{2+} transients, we measured somatic AP-evoked Ca^{2+} transients beyond proximal dendrites using OGB-1. Dendritic Ca^{2+} transients evoked by single APs or AP trains are not limited to regions close to the soma. The amplitude and decay of $[Ca^{2+}]_i$ associated with backpropagating APs are relatively independent of the distance from the soma. In sum, O-LM cells exhibit low endogenous Ca^{2+}-binding ratios and relatively distance-independent Ca^{2+} dynamics in the dendrites. These special features of Ca^{2+} signaling in O-LM cells may have important functional implications for both normal and pathological conditions.

Key words: GABAergic interneuron, Ca^{2+} binding ratio, fura-2, dendrite, Ca^{2+} imaging.

*Corresponding author. Tel: +886-2-2826-7325; fax: +886-2-2821-5307.
E-mail address: cclien@ym.edu.tw (C. C. Lien).

Abbreviations: AMPAR, α-amino-3-hydroxy-5-methyl-4-isoxazolepropionic acid receptor; bAPs, backpropagating action potentials; BC, basket cell; GluR, glutamate receptor; LTD, long-term depression; LTP, long-term potentiation; OGB-1, Oregon Green BAPTA-1; O-LM cell, oriens lacunosum-moleculare cell; ROI, region of interest; STDP, spike timing-dependent plasticity; VGCCs, voltage-gated Ca^{2+} channels.

Quantitative features of Ca^{2+} homeostasis in the neuronal cytoplasm are important because they determine the spatiotemporal profile of Ca^{2+} signaling that controls the development, plasticity, regeneration, and cell death in the nervous system (Zheng and Poo, 2007; Neher, 2008). These features include the dynamics of Ca^{2+} sources, Ca^{2+} buffering and diffusion. Intracellular Ca^{2+} buffering systems consist of Ca^{2+}-binding proteins, plasma membrane extrusion, and sequestration into intracellular organelles (Pottorf et al., 2000; Hartmann and Konnerth, 2005; Müller et al., 2007; Scheuss et al., 2006; Stocca et al., 2008). Although the spatiotemporal profile of dendritic Ca^{2+} dynamics varies greatly among different types of neurons (Lee et al., 2000; Kaiser et al., 2001; Goldberg et al., 2003, 2004; Goldberg and Yuste, 2005; Rozsa et al., 2004; Aponte et al., 2008), accumulating evidence supports the prevalent view that γ-aminobutyric acid-releasing (GABAergic) interneurons possess higher Ca^{2+} buffer capacities than those of principal neurons (Lee et al., 2000; Rozsa et al., 2004; Goldberg and Yuste, 2005; Aponte et al., 2008).

GABAergic interneurons consist of a heterogeneous population of cells (reviewed by Klausberger and Somogyi, 2008). At least two classes of functionally distinct interneurons are known to exist in the hippocampus (McBain and Fisahn, 2001; Jonas et al., 2004). Somatic inhibitory interneurons, such as fast-spiking basket cells (BCs), control the spike initiation of principal neurons via axonal innervations onto perisomatic areas of principal neurons (Cobb et al., 1995; Miles et al., 1996; Kraushaar and Jonas, 2000), whereas dendritic inhibitory interneurons, such as oriens lacunosum-moleculare (O-LM) cells, regulate dendritic Na^+ or Ca^{2+} spikes and synaptic plasticity by innervating dendritic domains of principal neurons (Miles et al., 1996; Pouille and Scanziani, 2004). These two distinct interneuron subtypes differ not only in their intrinsic properties, such as neurochemical contents, Ca^{2+}-binding proteins, ion channels, and transmitter receptors (Koh et al., 1995; Freund and Buzsáki, 1996; Martina et al., 1998; Lien et al., 2002; Pouille and Scanziani, 2004; Aponte et al., 2006), but also in their synaptic and network functions (Pouille and Scanziani, 2004; Klausberger et al., 2003; Klausberger and Somogyi, 2008). A recent study showed that fast-spiking parvalbumin-expressing BCs in the dentate gyrus exhibit efficient Ca^{2+} buffer capacity in the proximal dendrites (Aponte et al., 2008). In contrast to BCs and other types of GABAergic interneurons (Kaiser et al., 2001; Goldberg et al., 2003, 2004; Goldberg and Yuste, 2005; Rozsa et al., 2004), the Ca^{2+} handling properties of O-LM

0306-4522/09 $ - see front matter
doi:10.1016/j.neuroscience.2009.09.052

cells, a major type of dendritic inhibitory interneurons in the hippocampus, remain unexplored.

Understanding the Ca^{2+} buffering and Ca^{2+} load in distinct types of interneurons may be helpful for understanding the selective resistance or vulnerability of these neurons under pathophysiological conditions (Morin et al., 1998; Cossart et al., 2001; Sloviter et al., 2003). For instance, dendritic inhibitory interneurons (e.g., O-LM cells), but not somatic inhibitory interneurons (e.g., BCs in the CA1 region), preferentially degenerate in experimental temporal lobe epilepsy (Morin et al., 1998; Cossart et al., 2001; Maglóczky and Freund, 2005). Although the exact mechanism of this cell loss is unknown, accumulating evidence points to Ca^{2+} overload as the cause of differential vulnerability of O-LM cells (Woodhall et al., 1999; Gee et al., 2001). However, Ca^{2+} buffer capacity and changes of Ca^{2+} concentrations during spiking activities in O-LM cells remain unknown.

In this study, we combined whole-cell patch-clamp recording with ratiometric Ca^{2+} imaging at the dendrites using high-affinity Ca^{2+} indicators fura-2 and Oregon Green BAPTA-1 (OGB-1). A major goal of this study was to determine the endogenous Ca^{2+}-binding ratio and the AP-evoked Ca^{2+} concentrations in the absence of exogenous buffers in the proximal dendrites. A second major goal was to determine the spatial profile of dendritic Ca^{2+} transients evoked by backpropagating action potentials (bAPs) along the dendrites of O-LM cells. Our results revealed that O-LM cells have low endogenous Ca^{2+}-binding ratios which may contribute to the large $[Ca^{2+}]_i$ transients during APs. In addition, Ca^{2+} accumulation in the dendrite of O-LM cells during bAPs is relatively independent of the distance from the soma.

EXPERIMENTAL PROCEDURES

Preparation of hippocampal slices

Transverse hippocampal slices (300–350 μm thick) were prepared from male Sprague–Dawley rats [postnatal day 16 (P16)-P21] using a vibrating tissue slicer (DSK-1000, Dosaka, Kyoto, Japan) as described previously (Lien et al., 2002; Lien and Jonas, 2003). Animals were sacrificed by rapid decapitation without anesthesia in accordance with national and institutional guidelines. Experiments were approved by the Animal Care and Use Committee of National Yang-Ming University. Slices were sectioned in ice-cold artificial cerebrospinal fluid (ACSF) containing (in mM): 125 NaCl, 25 $NaHCO_3$, 1.25 NaH_2PO_4, 2.5 KCl, 25 glucose, 2 $CaCl_2$, 1 $MgCl_2$. Following sectioning, slices were incubated in a holding chamber filled with the oxygenated (95% O_2−5% CO_2) solution containing (in mM): 87 NaCl, 25 $NaHCO_3$, 1.25 NaH_2PO_4, 2.5 KCl, 10 glucose, 75 sucrose, 0.5 $CaCl_2$, 7 $MgCl_2$ at 34 °C for 25 min, and then at room temperature until used. During experiments, an individual slice was transferred to a submersion recording chamber and was continuously superfused with ACSF, bubbled with 95% O_2−5% CO_2.

Electrophysiology

Patch pipettes for recordings were pulled from borosilicate glass tubing (outer diameter 1.5 mm, inner diameter 0.86 mm; Harvard Apparatus, Holliston, MA, USA) and heat-polished before use. The pipette resistance ranged from 2 to 6 MΩ. Experiments were performed under visual control using an infrared differential interference contrast (IR–DIC) microscope (BX51WI, Olympus, Tokyo, Japan). O-LM cells in the stratum oriens/alveus of CA1 region were visually identified by the fusiform cell bodies and two horizontally oriented dendrites (Lien et al., 2002; Lien and Jonas, 2003). Cells exhibited pronounced sag responses during 1 s hyperpolarizing current pulse injection and modest fast-spiking patterns (~50 Hz) upon injection of depolarizing current pulses were used for further recording. Patch-clamp whole-cell recordings were made as described previously (Lien and Jonas, 2003; Lien et al., 2006), using a Multiclamp 700 B amplifier (Molecular Devices, Union City, CA, USA). Pipette capacitance and access resistance (10–30 MΩ) were compensated. Single APs in short bursts were evoked by single current pulses of 2 ms, with 2–3 nA. Oscillatory spikes were evoked by 5 Hz sinusoidal (8 s, 250–450 pA peak to peak) current pulses. Signals were low-pass filtered at 4 kHz (four-pole Bessel), and sampled at 10 kHz using a Digidata 1440 (Molecular Devices); data acquisition and pulse generation were performed using pClamp 10.2 (Molecular Devices). Recordings were made at 22–25 °C.

Fluorescence measurements with fura-2 and OGB-1

Ca^{2+} concentrations were measured using dual wavelength ratiometric method (Grynkiewicz et al., 1985). A polychromatic illumination system (polychrome V with 150 W Xenon lamp, bandwidth ~13 nm, TILL Photonics GmbH, Gräfelfing, Germany) was coupled to the epi-fluorescent port (BX-RFA, Olympus) of the microscope (Olympus BX51WI with a 60× water immersion objective, Olympus, Tokyo, Japan) via a quartz light guide and an epi-fluorescence condenser. The system provides fast switching (<1 ms) between the excitation wavelength (380 nm) and the Ca^{2+}-insensitive (isosbestic) excitation wavelength for fura-2 (362 nm in our system, comparable to 360 nm used by Neher and Augustine, 1992). Light intensity was attenuated by 75% using a neutral density filter (ND-25, Olympus, Tokyo, Japan) to reduce bleaching of the fluorescence dyes. The filter combination for excitation and emission consisted of a beam splitter (400DCLP, Chroma Technology Corp., Rockingham, VT, USA) and a long-pass emission filter (E420LPv2, Chroma Technology Corp). To investigate the spatial profile of dendritic $[Ca^{2+}]_i$ along dendrites, we used OGB-1 instead of fura-2 illuminated by a single wavelength of 494 nm through a filter combination for excitation and emission consisting of a dichroic mirror (DM505, Olympus, Tokyo, Japan) and a barrier filter (BA510IF, Olympus, Tokyo, Japan). Fluorescence was measured with a 16-bit frame-transfer electron-multiplying charged-coupled device (EM-CCD) camera (QuantEM 512SC, Photometrics, 10 MHz read out, a pixel size of 16 μm). The monochromator and image acquisition were controlled by a PC running MetaFluor software (Molecular Devices).

Images with full spatial resolution (512×512 pixel sizes) were taken with exposure times up to 2.5 s. For high-speed Ca^{2+} measurement (≥95 Hz), a rectangular region of interest (ROI), typically 2.7×5.3 μm (~10×20 pixel sizes), was defined over the proximal dendrites of O-LM cells at a distance of about 20 μm from soma (Fig. 1D). Fluorescence measurements were initiated 20 min after whole-cell recording was obtained, with the exception of the loading curve experiments (Fig. 2A) in which measurements were started before and immediately after break-in. Fluorescence traces had duration of 10–20 s and were separated by intersweep intervals of 20–40 s. Signals were corrected for background, which was obtained from a second ROI with identical size but shifted by 22–24 μm perpendicularly to the dendritic axis in comparison to the original ROI. Changes in background-subtracted fluorescence were expressed as $\Delta[Ca^{2+}]_i$ for fura-2 experiments or $\Delta F/F\% = [(F - F_{rest})/F_{rest}] \times 100\%$ for OGB-1/−5 N experiments.

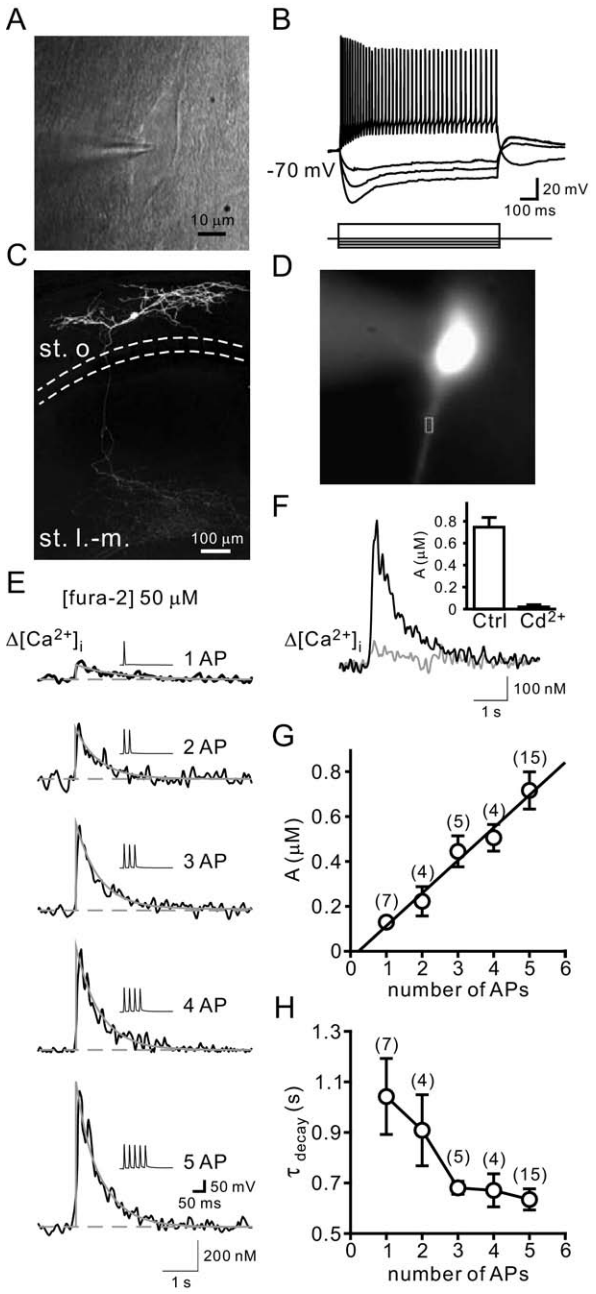

Fig. 1. AP-evoked Ca^{2+} transients of O-LM cells in the CA1 region of rat hippocampus (A) IR-DIC video image of an O-LM cell in the stratum oriens of CA1 region. A recording pipette was shown on the left side. (B) Voltage responses to 1 s de- or hyperpolarizing current pulses in the whole-cell current clamp recording configuration. Current during the pulse −300, −200, −100 and +500 pA. Membrane potential before the pulse was −70 mV. (C) A two-photon *z*-stack (maximal intensity) projection of the same O-LM cell in (B) spanning a depth of 97 μm. Cell was filled with biocytin during whole-cell recording and stained with Alexa 488-conjugated avidin. Dashed lines denote borders of the stratum pyramidale. The soma and dendrites are located in the stratum oriens (st. o) and the axonal innervations are confined to the stratum lacunosum-moleculare (st. l.-m.). (D) Fluorescence image of an O-LM cell (excitation wavelength 362 nm) and the attached pipette (left) containing 50 μM fura-2. Square indicates the region of interest (ROI) used for Ca^{2+} measurements. (E) Ca^{2+} transients evoked by a single AP or 100 Hz bursts of two, three, four and five APs. Traces are averages of 5 to 10 sweeps. (F) Representative AP-evoked Ca^{2+} transients before (Ctrl) and after addition of Cd^{2+} (200 μM), a broad-spectrum VGCC blocker. Inset showed the average of total three cells. (G) Plot of peak amplitude of Ca^{2+} transients (measured by 50 μM fura-2) against the number of APs. Data were fitted with a linear function $y=0.1456\times-0.0328$, yielding a slope of 145.6 nM AP^{-1} ($r^2=0.94$). Numbers of measurements are given in parentheses above data points. (H) Plot of decay time constant of Ca^{2+} transients against the number of APs. Decay rates were accelerated with increasing numbers of APs.

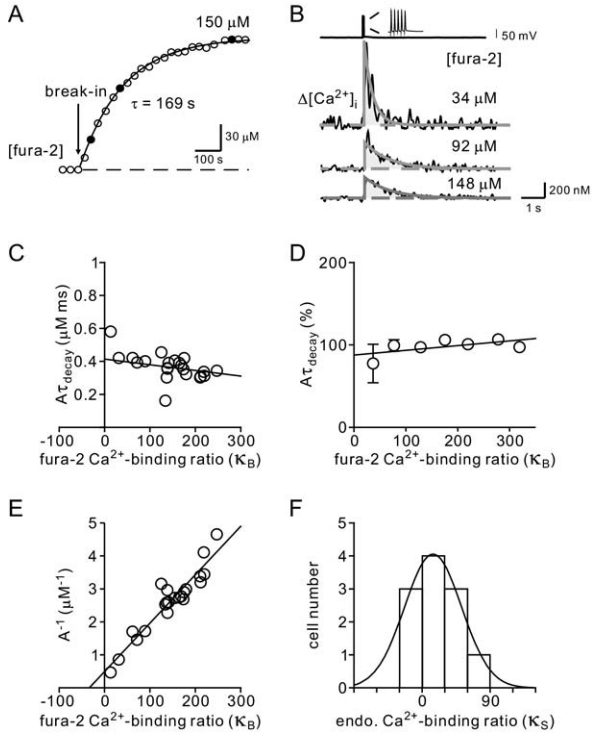

Fig. 2. Estimates of endogenous Ca^{2+}-binding ratio during fura-2 loading process (A) Fura-2 loading after break-in was monitored by measuring background subtracted isosbestic fluorescence intensities, assuming full loading after the fluorescence reached a plateau level. Fluorescence signals were converted to fura-2 concentrations; fura-2 concentration of each black circle was shown in (B). (B) Dynamics of Ca^{2+} transients is dependent on fura-2 concentrations. Amplitudes of Ca^{2+} transients became smaller with increasing fura-2 concentrations, while the decay time constants increased. Decay was fitted with an exponential function. Gray area represents the integral of $A\tau_{decay}$. (C) Plot of the products of the peak amplitude A and τ_{decay} of transients against fura-2 κ_B of an O-LM cell. The solid line represents a linear regression to the mean data ($r^2=0.03$). (D) Summary plot of $A\tau_{decay}$ against the fura-2 κ_B from a total of 14 cells. The solid line represents a linear regression to the mean data ($r^2=0.37$). (E) Plot of the A^{-1} against κ_B of an O-LM cell, yielding κ_S of 33. The solid line represents a linear regression to the mean data ($r^2=0.90$). (F) Histograms showing the κ_S values determined by A^{-1} from 11 anatomically identified O-LM cells. Distribution of data was fitted with a Gaussian function with the mean of 15 and SD of 38.

Calibration of the Ca^{2+} measurement

Fluorescence signals were converted into Ca^{2+} concentrations ($[Ca^{2+}]_i$) using isosbestic rationing (Neher and Augustine, 1992). The AP-evoked fluorescence change was recorded at an excitation wavelength of 380 nm while the isosbestic fluorescence was

measured using the Ca^{2+}-insensitive excitation wavelength (362 nm under our condition). The ratio of fluorescence signal was calculated according to $R=(F_{362}-B_{362})/(F_{380}-B_{380})$, with F_{362} and F_{380} the fluorescence signals at 362 and 380 nm, respectively and B_{362} and B_{380} the corresponding background signals acquired at a nearby region. The fluorescence ratio was converted into $[Ca^{2+}]_i$ using eqn. 1 (taken from Grynkiewicz et al., 1985):

$$[Ca^{2+}]_i=K_{eff}((R-R_{min})/(R_{max}-R)) \quad (1)$$

With the effective dissociation constant $K_{eff}=K_d$ (R_{max}/R_{min}), where K_d is the indicator's dissociation constant for Ca^{2+}, R_{min} is the ratio in Ca^{2+}-free solution and R_{max} is the ratio when Ca^{2+} indicator is completely saturated with Ca^{2+}. These values were determined from O-LM cells. Briefly, O-LM cells were loaded via low access resistance pipette (≤12.5 MΩ) with intracellular solutions containing either 20 mM EGTA (Ca^{2+} free), 20 mM $CaCl_2$ (maximal Ca^{2+}) or a mixture of 7.06 mM CaEGTA and 2.94 mM EGTA (Ca^{2+} calibration kit, Invitrogen, Carlsbad, CA, USA), resulting in a free $[Ca^{2+}]_i$ of 400 nM. Using these solutions, the values for fura-2 were $R_{min}=0.72\pm0.01$ ($n=11$), $R_{max}=3.70\pm0.21$ ($n=5$) and $R_{400}=1.25\pm0.05$ ($n=6$). These results gave K_d of 360 nM, which is almost ~2-fold larger than the value determined *in vitro* (161 nM, Kao and Tsien, 1988), consistent with a previous report that K_d in cytoplasm may be two-to eightfold larger than the *in vitro* values (Zhao et al., 1996). We are also aware that the K_d value determined from O-LM cells in our system was 1.2-fold larger than the value determined in other cell types (Kaiser et al., 2001; Aponte et al., 2008), but this would only influence our estimate of κ_s by a factor of <1.4 (Helmchen et al., 1996, 1997).

Determination of Ca^{2+}-binding ratio in single neurons

To estimate the Ca^{2+}-binding ratio, we treated the proximal dendrite as a single homogeneous compartment, assuming that Ca^{2+} inflow in the proximal dendrite is instantaneous and reaction between Ca^{2+} and buffers is rapid (Neher and Augustine, 1992; Helmchen et al., 1996, 1997; Helmchen and Tank, 2005; Aponte et al., 2008). The Ca^{2+}-binding ratio is constant and is defined as the ratio of the change in buffer-bound Ca^{2+} over free Ca^{2+} change after AP-evoked Ca^{2+} inflow (Neher and Ausgustine, 1992; Helmchen and Tank, 2005):

$$\kappa_S=\frac{\Delta[SCa^{2+}]}{\Delta[Ca^{2+}]} \quad (2)$$

$$\kappa_B=\frac{\Delta[BCa^{2+}]}{\Delta[Ca^{2+}]} \quad (3)$$

S and B represent for endogenous (S) and exogenous (B) buffers, respectively.

According to the law of mass reaction: $[Ca^{2+}]+[B]\rightleftharpoons[BCa^{2+}]$, we can derive eqn. 4.

$$[BCa^{2+}]=\frac{B_T[Ca^{2+}]}{[Ca^{2+}]+K_d} \quad (4)$$

where B_T and K_d are total concentration of buffer B and dissociation constant for buffer B, respectively.

Therefore,

$$\Delta[BCa^{2+}]=[BCa^{2+}]_{peak}-[BCa^{2+}]_{rest}=\frac{B_T[Ca^{2+}]_{peak}}{[Ca^{2+}]_{peak}+K_d}-\frac{B_T[Ca^{2+}]_{rest}}{[Ca^{2+}]_{rest}+K_d} \quad (5)$$

Equation 5 can be further rearranged as eqns. (6) and (7)

$$\Delta[BCa^{2+}]=\frac{B_TK_d([Ca^{2+}]_{peak}-[Ca^{2+}]_{rest})}{([Ca^{2+}]_{peak}+K_d)([Ca^{2+}]_{rest}+K_d)}$$

$$=\frac{B_TK_d\Delta[Ca^{2+}]}{([Ca^{2+}]_{peak}+K_d)([Ca^{2+}]_{rest}+K_d)}$$

$$\kappa_B=\frac{\Delta[BCa^{2+}]}{\Delta[Ca^{2+}]}=\frac{B_TK_d}{([Ca^{2+}]_{peak}+K_d)([Ca^{2+}]_{rest}+K_d)} \quad (7)$$

Single compartment model of dendritic Ca^{2+} buffering

A single compartment model as described by Neher and Augustine (1992) was used to estimate the endogenous Ca^{2+}-binding ratio. The model assumes that AP-evoked Ca^{2+} inflow (total charge Q_{Ca}) in the proximal dendrite (the volume V) is instantaneous and rapidly reaches equilibrium with buffers. The total Ca^{2+} load ($\Delta[Ca^{2+}]_T$) upon initiation of APs in the proximal dendrite is $\Delta[Ca^{2+}]_{T,max}$, which is the sum of unbound and bound forms of Ca^{2+}, that is $\Delta[Ca^{2+}]_i+\Delta[SCa^{2+}]+\Delta[BCa^{2+}]$.

$$\Delta[Ca^{2+}]_{T,max}=\frac{Q_{Ca}}{2FV}=\Delta[Ca^{2+}]_i+\Delta[SCa^{2+}]+\Delta[BCa^{2+}] \quad (8)$$

$$\Delta[Ca^{2+}]_{T,max}=\frac{Q_{Ca}}{2FV}=\Delta[Ca^{2+}]_i\left(1+\frac{\Delta[SCa^{2+}]}{\Delta[Ca^{2+}]_i}+\frac{\Delta[BCa^{2+}]}{\Delta[Ca^{2+}]_i}\right)$$

$$=\Delta[Ca^{2+}]_i(1+\kappa_S+\kappa_B) \quad (9)$$

Where F is faraday's constant. With $A=\Delta[Ca^{2+}]_i$, eqn. 9 can be rearranged as

$$A^{-1}=\frac{(1+K_S+K_B)}{[Ca^{2+}]_{T,max}} \quad (10)$$

Thus, A^{-1} plotted against κ_B should follow a straight-line, which intercepts the horizontal axis at $-(1+\kappa_S)$. Using this relationship, the endogenous Ca^{2+}-binding ratio κ_S can be estimated by measuring A, the AP-evoked $\Delta[Ca^{2+}]_i$ with different concentrations of fura-2 (corresponding to different values for κ_B according to eqn. 7. Furthermore, the amplitude of Ca^{2+} transient in the absence of fura-2 can be obtained by extrapolation to $\kappa_B=0$.

Here we shall carefully interpret the meaning of κ_S. The model arbitrarily divides the buffering systems into fast and slow buffering systems. The AP-evoked Ca^{2+} inflow is assumed to be instantaneous in the proximal dendrites (like a δ function) and reach equilibrium with the fast buffers. On the other hand, the return of intracellular $[Ca^{2+}]_i$ to baseline levels following peak amplitude of $[Ca^{2+}]_i$ is assumed to be mediated by a variety of extrusion mechanisms. However, those assumptions ignore the possible interaction and overlapping of two buffering systems. Therefore, although the κ_S is termed endogenous Ca^{2+}-binding ratio in this study, it reflects a lumped value for endogenous fast mobile buffers, fast fixed buffers and parts of relatively slow buffering mechanisms.

Solutions and drugs

The intracellular solution for recording pipettes consisted of (in mM): 125 potassium gluconate, 4 $MgCl_2$, 4 K_2ATP, 10 Hepes, 10 Na_2-phosphocreatine, 0.3 Na_3GTP, different concentrations of Ca^{2+} indicators and 0.2% biocytin (pH adjusted to 7.3 with HCl). Ca^{2+} indicators fura-2, OGB-1 and OGB-5N were from Invitrogen (Eugene, OR, USA). All other chemicals were from Sigma (St. Louis, MO, USA) except where noted.

Post hoc identification of O-LM cell morphology

Neurons were filled with biocytin (2 mg/ml) during whole-cell recordings and subsequently fixed overnight with 4% paraformaldehye in phosphate-buffered solution (PB; 0.1 M, pH 7.3). After washing with PB, slices were incubated with fluorescein isothiocyanate (FITC) or Alexa 488-conjugated avidin-D (2 μl/ml; Invitro-

gen, Eugene, OR, USA) in PB and 0.3% triton X-100 overnight at 4 °C. After wash, slices were embedded in mounting medium Vectashield® (Vector Laboratories, Burlingame, CA, USA). Labeled O-LM cells were examined by a two-photon microscope using a pulsed titanium: sapphire laser (Chameleon-Ultra II tuned to 800 nm; Coherent, Portland, OR, USA) attached to a Leica DM6000 CFS (Leica, Wetzlar, Germany) that was equipped with a 20×/1.0 numerical aperture (NA) water immersion objective (HCX APO L; Leica, Wetzlar, Germany). The morphology of the cells was reconstructed from a stack of up to 152 images (voxel size, 0.378 μm in the x-y plane; 1 μm along the z-axis).

Data analysis and statistics

Data were analyzed using Clampfit 10.2 (Molecular Devices), Mathematica (version 6.0, Wolfram, Champaign, IL, USA), and GraphPad Prism (version 5.0, La Jolla, CA, USA). The measurement of peak amplitude (A) and decay time constant (τ_{decay}) draws on the single compartment model in which the $[Ca^{2+}]_i$ transient is described by an instantaneous rise and an exponential decay (Helmchen et al., 1996). In the present study, we fitted the decay time course of Ca^{2+} transients with mono- and bi-exponential functions. A mono-exponential fit was preferred because in many cases the time constants of the fast components were very small and resulted in enormously large values of A (see below). To obtain A, we extrapolated the fitted mono-exponential function to the time point of the Ca^{2+} signal rise (Helmchen et al., 1996). The time point is defined by the first sampling point that is greater than 3 or 4 standard deviation of baseline $[Ca^{2+}]_i$ values and is close to the midpoint of the rising phase (Fig. 1E; Helmchen et al., 1996).

Values indicate mean±SEM if not otherwise stated. Error bars in figures also represent SEM. Statistical significance was tested by the non-parametric Mann–Whitney or Kruskal-Wallis tests at the significance level (P) indicated, using GraphPad Prism 5.0 (La Jolla, CA, USA).

RESULTS

Ca^{2+} imaging of dendrite-targeting O-LM cells

APs propagate reliably into horizontally oriented dendrites of O-LM cells (Martina et al., 2000). To examine Ca^{2+} concentrations and buffering during AP backpropagation in the dendrite of these neurons, we loaded the cell with biocytin and high-affinity Ca^{2+} indicators fura-2 or OGB-1 via the patch pipette during whole-cell recording. O-LM cells selected for Ca^{2+} imaging were based on the following criteria as previously described (Maccaferri et al., 2000; Lien et al., 2002; Lien and Jonas, 2003; Lawrence et al., 2006): (1) elongated soma and two horizontally oriented dendrites in the stratum oriens/alveus of the CA1 hippocampus, as viewed under the IR-DIC optics (Fig. 1A); (2) appearance of AP trains (up to 60 Hz) during 1 s depolarizing current pulses and marked “sag” responses during hyperpolarizing current pulses at 22 °C (Fig. 1B); (3) a modest AP frequency adaptation and AP amplitude accommodation during the AP train (Fig. 1B). Consistent with previous reports (Lien et al., 2002; Lawrence et al., 2006; Maccaferri, 2005), the large majority (75%) of neurons selected on the basis of these criteria displayed axon projections across the stratum pyramidale and dense axonal branches in the stratum lacunosum-moleculare after post hoc treatment with Alexa 488-conjugated avidin (Fig. 1C). Only neurons with axon projection in the stratum lacunosum-moleculare were used for subsequent analysis.

To ensure diffusion equilibration of the Ca^{2+} indicators, we chose a small dendritic region 20 μm from the soma (boxed region) for Ca^{2+} imaging after 20 min of fura-2 loading during whole-cell recording (Fig. 1D). The speed of dye loading as reflected by the fluorescence signals in the proximal dendrites clearly depended on access resistance. It is faster with lower access resistance. The average time constant of dye loading was 165±29 s in proximal dendritic regions from 11 cells, comparable to previous estimates (Helmchen et al., 1996). A representative loading curve was shown in Fig. 2A. After loading for at least 20 min (more than five-fold loading time constant; Fig. 1D), dendritic $[Ca^{2+}]_i$ transients were evoked by single APs and measured at an acquisition rate of 95 Hz (Fig. 1E; see Experimental procedures). Fluorescence signals evoked by a single AP or a burst of several APs (at 100 Hz) were converted into $[Ca^{2+}]_i$ using the isosbestic ratioing method according to eqn. 1 in Experimental procedures (Fig. 1E) that yielded the resting $[Ca^{2+}]_i$ was 22±5 nM (n=11). Both single APs and AP bursts led to rapidly rising $[Ca^{2+}]_i$ transients with a relatively slow decay. Consistent with a recent report that voltage-gated Ca^{2+} channels (VGCCs) are the major sources of Ca^{2+} influx during APs (Topolnik et al., 2009), AP-evoked Ca^{2+} transients in the control (Ctrl; 747±88 μM) were largely abolished by the bath presence of 200 μM Cd^{2+} (20±20 μM), a non-selective VGCC blocker (n=3; Fig. 1F). Further quantitative analysis of Ca^{2+} transients showed that amplitudes of Ca^{2+} transients were proportional to the number of spikes (the value of the slope is 146 nM/AP; Fig. 1G), whereas the decay time constants became faster with increased number of spikes (Fig. 1H). These results indicate that Ca^{2+} transients evoked by single APs summated linearly during 100 Hz bursts of APs. The acceleration of the decay, similar to those reported for some other preparation, strongly suggests that the Ca^{2+} clearance might not be constant, but rather depends on the $[Ca^{2+}]_i$ (Scheuss et al., 2006; Stocca et al., 2008).

Endogenous Ca^{2+}-binding ratio during fura-2 loading

To estimate the endogenous Ca^{2+}-binding ratio κ_S, we first quantified the amplitude and time course of $\Delta[Ca^{2+}]_i$ in proximal dendrites by loading single cells with exogenous Ca^{2+} buffer fura-2 (150 μM) and continuously monitored the fura-2 buffering effect on Ca^{2+} transients evoked by a 100 Hz train of five APs at the soma during loading. This approach is believed to minimize the possible “washout” of mobile buffers and reflects cell to cell variability because κ_S values were obtained from individual cells (Helmchen and Tank, 2005; Aponte et al., 2008). Fluorescence signals evoked by bursts of five APs at 100 Hz were measured every 20–40 s during the fura-2 loading. The fluorescence signals, reflecting the fura-2 concentration ($[fura\text{-}2]_i$), followed an exponential rise and finally reached a plateau. The fluorescence excitation was performed at the isosbestic wavelength 362 nm ($I_{362}=F_{362}–B_{362}$), which was insensitive to $[Ca^{2+}]_i$ but was proportional to $[fura\text{-}2]_i$. This signal was converted to $[fura\text{-}2]_i$, assuming that $[fura\text{-}2]_i$ in the proximal dendrites reached the concentration in

Table 1. Comparison of Ca^{2+} concentrations and buffering in proximal dendrites of O-LM and PCs

Parameter	O-LM	CA1 PC	*P*
Resting $[Ca^{2+}]_i$	22±5 nM (*n*=11)	15±4.6 nM (*n*=6)	0.72
κ_S from A^{-1}	20±8 (*n*=11)[a]	101±29 (*n*=6)[a]	<0.05
$[Ca^{2+}]_i$ amplitude/AP	656±226 nM (*n*=8)[b]	265±48 nM (*n*=6)[b]	0.28
Total $[Ca^{2+}]$ load/AP	11.9±0.3 μM (*n*=11)	19.4±1.9 μM (*n*=6)	<0.005

For comparison, both data groups were obtained by the loading curves under the same conditions.

[a] Standard error of the mean was calculated from all κ_S values obtained by separate analysis of each cell.

[b] Value was obtained by extrapolation to κ_B=0; negative values of intercept of y-axis were not included. Total $[Ca^{2+}]$ load is the sum of unbound and bound forms.

the pipette (150 μM; Fig. 2A). The AP-evoked Ca^{2+} transient depended on $[fura\text{-}2]_i$ during loading. As predicted by eqn. 10, Ca^{2+} transient amplitudes decreased with time, while their decay time constants increased during loading (Fig. 2B). The integral of Ca^{2+} transients $A\times\tau_{decay}$ weakly depended on κ_B (r^2=0.03 and r^2=0.37 for Fig. 2C, D, respectively), indicating again that Ca^{2+} clearance may not be constant. We thus determined the endogenous Ca^{2+} buffering by plotting the inverse of amplitude of Ca^{2+} transient, A^{-1} against κ_B and fitted them with a linear function. This yielded κ_S of 33 (r^2=0.89; Fig. 2E). Overall, the κ_S values obtained by *A* from 11 rigorously identified O-LM cells were normally distributed with an average value of 15 (Fig. 2F). For the quantitative comparison, the same experiments were performed in CA1 pyramidal cells (Supplementary Fig. 1; also see Table 1). The average κ_S value obtained from CA1 cells was 101±29 (*n*=6), comparable to previous estimates (Helmchen et al., 1996; Maravall et al., 2000), but significantly larger than that of O-LM cells ($P<0.05$; Mann–Whitney test).

Endogenous Ca^{2+}-binding ratio under fura-2 loading

Another alternative approach to estimate the endogenous Ca^{2+}-binding ratio κ_S is to quantify the amplitude of $\Delta[Ca^{2+}]_i$ in proximal dendrites (Fig. 3A) by recording Ca^{2+} transients after full loading of exogenous Ca^{2+} buffer fura-2 (50–200 μM). At the steady $[fura\text{-}2]_i$, Ca^{2+} transients rapidly reached a peak after trains of 5 APs at 100 Hz and then decayed relatively slowly (Fig. 3B). The amplitudes of $[Ca^{2+}]_i$ decreased, whereas the decay time constants increased with increasing $[fura\text{-}2]_i$ (Fig. 3C). For quantitative analysis, the proximal dendrite was treated as a single, homogeneous compartment (Neher and Augustine, 1992). The κ_B of fura-2 was determined by eqn. 7 by measuring resting and peak $[Ca^{2+}]_i$. According to the single compartment model (Neher and Augustine, 1992), the relation between A^{-1} and κ_B is expected to fall on a straight line. Thus, we plotted the A^{-1} of $[Ca^{2+}]_i$ against κ_B and fitted the data with a linear function (r^2=0.98; Fig. 3D). According to eqn. 10, the intercept of x-axis equals $-(1+\kappa_S)$, where κ_S represents the endogenous Ca^{2+}-binding ratio and is about 27 (Fig. 3D).

AP-evoked dendritic Ca^{2+} dynamics beyond proximal dendrites

To investigate the Ca^{2+} dynamics beyond proximal dendrites, we imaged the Ca^{2+} influx by switching to the Ca^{2+} indicator OGB-1. Because OGB-1 signals ($\Delta F/F$ ~0.4) in response to single APs is about eight-fold larger than fura-2 signals ($\Delta F/F$ ~0.05), it is more suitable for detecting Ca^{2+} influxes in small neuronal compartments, such as oblique or distal dendrites (Yasuda et al., 2004; Kampa and Stuart, 2006; Topolnik et al., 2009). A montage of epi-fluorescence images along the horizontal dendrites of an O-LM cell is shown in Fig. 4A. Trains of five APs at 100 Hz were induced by somatic current injection (Fig. 4B, top). The fluorescence signals were acquired at several selected ROIs along the somato-dendritic axis (Fig. 4B). The fluorescence signals associated with single APs or a burst of five APs at 100 Hz slightly decreased with the distance from the soma (Fig. 4C; r^2 for black and gray lines were 0.02 and 0.02, respectively), consistent with a recent report by Topolnik et al. (2009). The kinetics of Ca^{2+} transients, such as decay time constants (r^2 for black and gray lines were 0.002 and 0.004, respectively) and 10–90% rise times (r^2 for black and gray lines were 0.08 and 0.02, respectively) were not correlated with the distance from the soma (Fig. 4D, E).

Dendritic Ca^{2+} signal during oscillatory activity patterns

O-LM cells generate APs with high frequency during theta oscillation in the behaving animal (Csicsvari et al., 1999; Klausberger and Somogyi, 2008). During the gamma rhythm, O-LM cells also fire preferentially at theta frequencies (Gloveli et al., 2005). Therefore, we measured Ca^{2+} signaling during such physiologically relevant protocols by applying 5 Hz sinusoidal (8 s, 250–550 pA peak to peak) current injection. To examine Ca^{2+} signaling up to the distal part of dendrite and avoid dye saturation during oscillatory spiking, we loaded cells with the low-affinity Ca^{2+} indicator OGB-5N (100 μM). During theta activities, O-LM cells fired doublets per cycle (Fig. 5A). The mean plateau values of Ca^{2+} signal ($\Delta F/F$) during the last 2 s theta stimulation measured in the proximal (18±1 μm), middle (96±9 μm) and distal (181±19 μm) dendrites of O-LM cells were 20±2%, 19±3% and 14±3%, respectively. The Ca^{2+} signaling during theta activity is relatively uniform along the somato-dendritic axis of O-LM cells (n=5, P=0.24 among three groups; Kruskal–Wallis test; Fig. 5B, D). Hippocampal CA1 pyramidal cells also showed firing preference at theta frequencies. However, in contrast to O-LM cells, oscillatory Ca^{2+} signaling in the pyramidal cell dendrite decreased markedly with distance from the

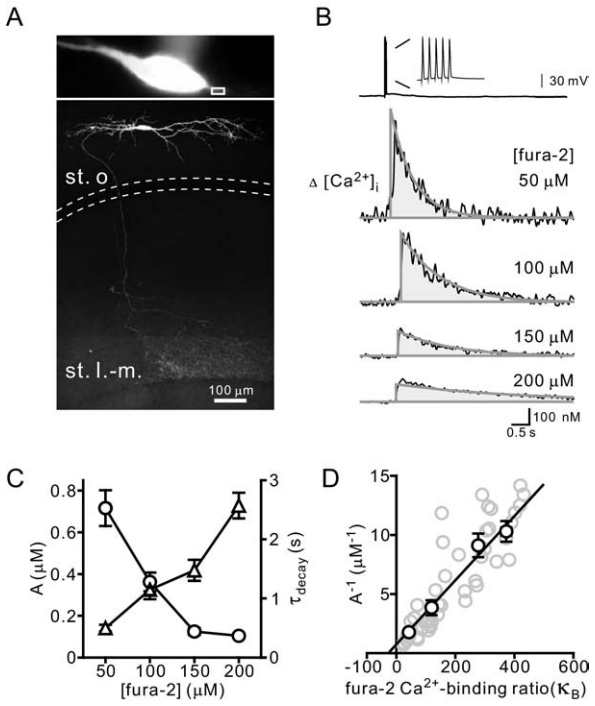

Fig. 3. Estimates of endogenous Ca^{2+}-binding ratio under steady-state concentration of fura-2 (A) Top, fluorescent image of an O-LM cell during loading of a fluorescent dye fura-2; a rectangle at the proximal dendrite indicates ROI for Ca^{2+} imaging. Bottom, an O-LM cell in the stratum oriens of CA1 region recovered after whole-cell recording and processed with fluorescently labeled avidin against intracellularly loaded biocytin. Dashed lines depict the borders of the stratum pyramidale. (B) $[Ca^{2+}]_i$ transients (bottom traces) evoked by bursts of 5 APs at 100 Hz (top), measured in the proximal dendrites of four different O-LM cells. Cells were somatically loaded with different fura-2 concentrations as indicated on the right. Measurements were performed during steady-state loading of fura-2. Each trace is an average of five sweeps. Exponential curves were fitted to the decays of the transients (time constants of 640, 1108, 1500, and 3457 ms, respectively). Gray area represents the integral $A\tau_{decay}$, the product of peak amplitude A, and time constant τ_{decay}. (C) Peak amplitude A (open circles) of $[Ca^{2+}]_i$ transients evoked by bursts of five APs at 100 Hz in the proximal dendrites of O-LM cells depends on fura-2 concentrations. Transients were large and decayed rapidly with low concentrations of fura-2 and vice versa. τ_{decay} (open triangles) of $[Ca^{2+}]_i$ transients evoked by bursts of five APs at 100 Hz in the proximal dendrites of O-LM cells also depends on the fura-2 concentrations. (D) Plot of the A^{-1} against the fura-2 κ_B. Gray circles, data from 53 individual O-LM cells; black circles, plot of the mean values of κ_B for 50, 100, 150 and 200 μM fura-2. The solid line represents a linear regression to the black circles (r^2=0.98).

soma. The mean plateau value of dendritic Ca^{2+} signal during the last 2 s oscillatory activity in the proximal (16±1 μm), middle (105±5 μm) and distal (250±34 μm) regions were 41±2%, 34±3% and 20±2%, respectively and showed significantly different (n=6, P<0.05, Kruskal–Wallis test; Fig. 5C, D).

The integral of Ca^{2+} transient over time at proximal, middle and distal dendrites of O-LM cells during oscillatory activities are 161±12%, 140±22% and 106±20%, respectively. Although the time integral of Ca^{2+} signal slightly decreased with the distance from the soma, the difference was not significant among groups (n=5, P=0.13, Kruskal–Wallis test; Fig. 5E). In contrast, the time integral of dendritic Ca^{2+} signal of CA1 pyramidal cells during the same activities decreased markedly with the distance from the soma. The time integral of Ca^{2+} transient at proximal, middle and distal dendrites of CA1 pyramidal cells are 329±19%, 263±23% and 163±18%, respectively and showed significantly different (n=6, P<0.05; Kruskal–Wallis test; Fig. 5E).

DISCUSSION

Many studies reported that interneurons possess higher Ca^{2+} buffer capacities than those of principal neurons (Lee et al., 2000; Rozsa et al., 2004; Goldberg and Yuste, 2005; Aponte et al., 2008). Here, we show that O-LM interneurons, a major class of dendrite-targeting interneurons in the rat hippocampus have a low endogenous buffer capacity and relatively large $[Ca^{2+}]_i$ changes in response to activity. Notably, the κ_S values of O-LM cells are significantly smaller than those of CA1 proximal apical dendrites (Supplementary Fig. 1, Table 1) and other subtypes of interneurons (Lee et al., 2000; Kaiser et al., 2001; Goldberg et al., 2003, 2004; Goldberg and Yuste, 2005; Rozsa et al., 2004; Aponte et al., 2008).

Factors that influence κ_S measurements

The Ca^{2+}-binding ratio of O-LM cells appears to be more comparable with those of spines and presynaptic terminals (Sabatini et al., 2002; Jackson and Redman, 2003; Helmchen et al., 1997) rather than those of proximal dendrites of principal neurons and other types of interneurons (Lee et al., 2000; Goldberg and Yuste, 2005; Aponte et al., 2008; see also Table 1). The κ_S values measured in the present study were not due to differences in the Ca^{2+} calibration. We used two approaches (dynamic loading and population analysis) to estimate κ_S based on the κ_B of fura-2, which depends inversely on the chosen K_d of fura-2. However, this is unlikely to result in an uncertainty factor >1.4 (Helmchen et al., 1996). Differences in optical imaging apparatus are also unlikely to account for the low κ_S value of O-LM cells, because the κ_S values (101±29 by the same loading method, n=6; supplementary Fig. 1) measured in the proximal apical dendrites of CA1 pyramidal cells are very comparable to previous estimates by other groups (Helmchen et al., 1996; Maravall et al., 2000). In contrast to CA1 pyramidal cells, the relatively low Ca^{2+} buffer capacity of O-LM cells might be attributed to the lack of calbindin or uncharacterized buffers in the majority of O-LM cells.

Comparison to previous work

Our results show that Ca^{2+} buffering and concentrations of O-LM interneurons, a typical class of dendritic inhibitory interneurons, are distinct from those of fast-spiking basket cells, a major class of somatic inhibitory interneurons (Aponte et al., 2008). In contrast to basket cells, O-LM cells have low endogenous Ca^{2+}-binding ratios and large dendritic $[Ca^{2+}]_i$ changes at zero added buffers. The quantitative comparison of endogenous Ca^{2+}-binding capacity is as follows: O-LM dendrites (κ_S=20−27) < hippocampal

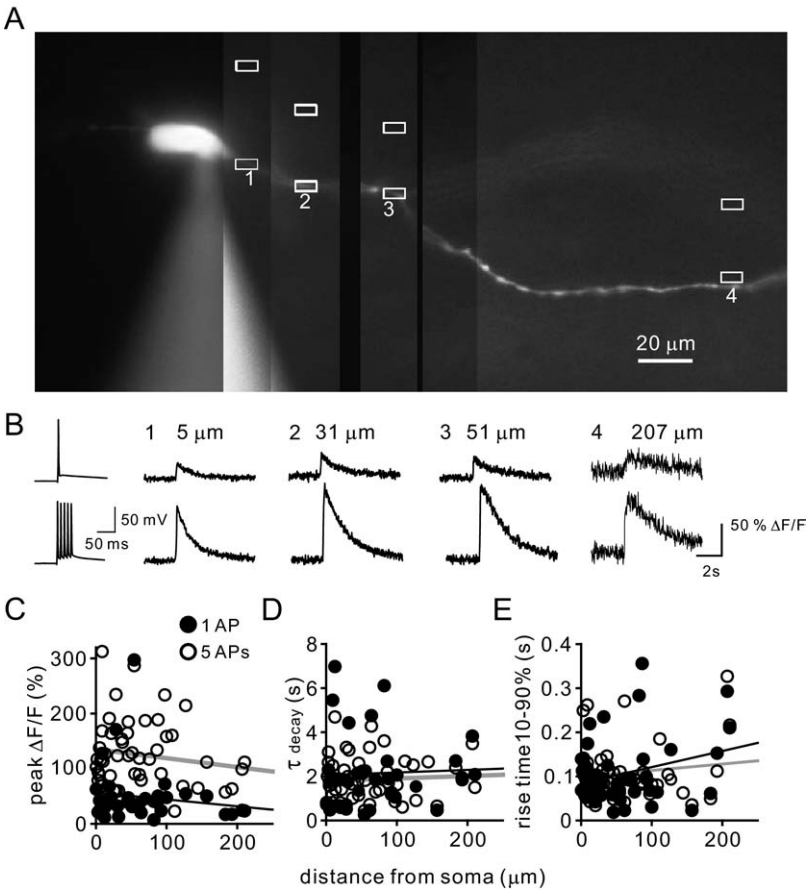

Fig. 4. Spatial profile of dendritic Ca^{2+} signaling during action potentials (A) Epi-fluorescence image of an O-LM cell loaded with the Ca^{2+}-sensitive dye OGB-1 (100 μM) via a patch pipette (left) during whole-cell recording. Locations of selected regions for Ca^{2+} measurement on a horizontal dendrite at different distances from the soma are indicated by rectangles and numbers. The image is a montage from several fluorescence images taken successively. The corresponding dendritic $[Ca^{2+}]_i$ transients evoked by either single APs or bursts of five APs at 100 Hz for each recording site are shown in (B). (B) Bursts of APs at 100 Hz were evoked at the soma and Ca^{2+} transients associated with single APs or trains of five APs at 100 Hz were taken at different sites of the dendrite indicated in (A). A representative burst of single and five APs at 100 Hz were shown on the left. (C) Ca^{2+} transients evoked by either a single AP (filled circles) or trains of five APs at 100 Hz (open circles) along the dendrites were independent of distances from the soma. The solid black and gray lines represent linear regressions to the filled (r^2=0.02) and open circles (r^2=0.02), respectively. (D) The decay time constants of Ca^{2+} transients evoked by either a single AP (black circles) or trains of five APs at 100 Hz (white circles). The solid black and gray lines represent linear regressions to the filled (r^2=0.002) and open circles (r^2=0.004), respectively. (E) The rise time (10–90%) of Ca^{2+} transients evoked by either a single AP (black circles) or trains of five APs at 100 Hz (white circles). The solid black and gray lines represent linear regressions to the filled (r^2=0.08) and open circles (r^2=0.02), respectively.

CA1 pyramidal neuron dendrites (κ_S=80−101, Table 1, supplementary Fig. S1; κ_S=64−186 by Helmchen et al., 1996; κ_S=44−80 by Maravall et al., 2000) <basket cell dendrites (κ_S=200; Aponte et al., 2008). Conversely, the peak amplitude of $[Ca^{2+}]_i$ at zero added buffers per AP showed: O-LM dendrites (A=241–613 nM) ≈ hippocampal CA1 pyramidal neuron dendrites (A=265 nM in this study, see Table 1 and Supplementary Fig. 1; A=150–240 nM by Helmchen et al., 1996; A=178–312 nM by Maravall et al., 2000) ≫ basket cell dendrites (A=50 nM; Aponte et al., 2008).

Ca^{2+} dynamics in distal dendrites of O-LM cells

Spatial profiles of Ca^{2+} influx during bAPs in the dendrites of GABAergic interneurons are diverse (Kaiser et al., 2001; Goldberg et al., 2003; Rozsa et al., 2004). Ca^{2+} imaging on dendrites of three types of V1 supragranular interneurons: parvalbumin-positive fast spikers, calretinin-positive irregular spikers, and adapting cells showed that calcium influx during backpropagation of AP trains was proximally restricted by potassium channels (Goldberg et al., 2003). The strong attenuation of Ca^{2+} influx is due to the failure of AP invasion into distal dendrites. In sharp contrast, back-propagating AP-evoked Ca^{2+} transients in dendrites of CA1 stratum radiatum interneurons underwent a distance-dependent increment (Rozsa et al., 2004). Between them, Ca^{2+} influx into the dendrites of bitufted interneurons in layer 2/3 of rat somatosensory cortex is relatively distance-independent (Kaiser et al., 2001).

Dendritic properties of O-LM cells are similar to those of bitufted interneurons in layer 2/3 because somatic APs of O-LM cells can actively and reliably propagate along the horizontal dendrites (Martina et al., 2000). Like bitufted interneurons, dendritic Ca^{2+} transients of O-LM cells are

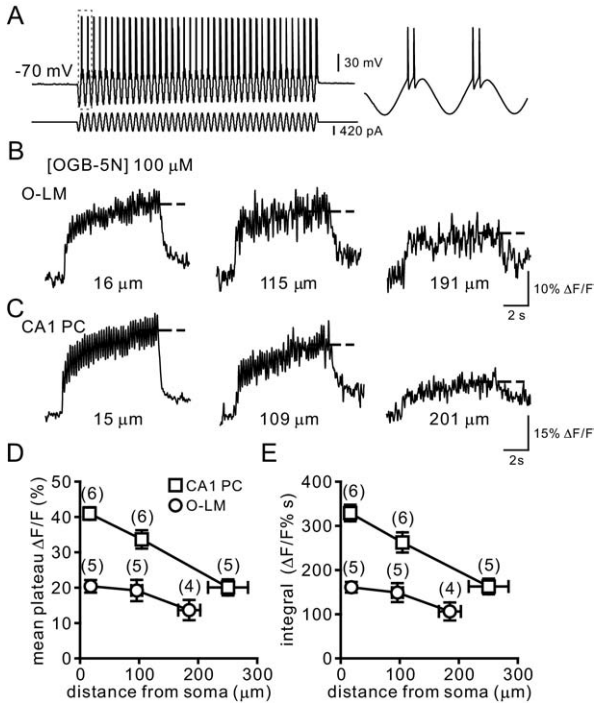

Fig. 5. Dendritic Ca^{2+} dynamics during oscillatory activities (A) Representative voltage response (top) of an O-LM cell to an 8 s, 420 pA sinusoidal (5 Hz) current injection (bottom). Expanded doublet spikes during the first and second cycles (right top). Membrane potential before the pulse was −70 mV. (B) Ca^{2+} transients during oscillatory activities were measured from the proximal (16 μm), middle (115 μm), and distal (191 μm) dendrites of an O-LM cell. Oscillatory Ca^{2+} signal decreased slightly with the distance from the soma. (C) Oscillatory Ca^{2+} signaling measured from different regions of the apical dendrite of a CA1 pyramidal cell. Amplitude of dendritic Ca^{2+} signal decreased markedly with the distance from the soma. Traces of Ca^{2+} transients in (B) and (C) are averages of 5 to 10 individual sweeps. Data were obtained from cells filled with 100 μM OGB-5N. Dashed lines indicate the mean value of the plateau during the last 2 s theta stimulation. (D) Plot of mean plateau value of Ca^{2+} signal (ΔF/F) during the last 2 s theta stimulation against the distance from the soma. (E) Plot of integral of Ca^{2+} signal (ΔF/F% s) over time against the distance from the soma.

not limited to the regions near the somata. The dendritic Ca^{2+} transients are relatively independent of distance from the somata (r^2=0.02 for both single AP and 5 APs; Fig. 4C; similar to Topolnik et al., 2009). However, unlike bitufted interneuron, the endogenous Ca^{2+}-binding ratio of O-LM cells (κ_S=19−27) is about 10-fold lower than that (~285) of bitufted interneurons in layer 2/3. Therefore, the peak amplitude of dendritic Ca^{2+} concentration per AP is likely larger than that of bitufted interneurons. Indeed, dendritic $[Ca^{2+}]_i$ (656±226 nM per AP) of O-LM cells is larger than that (136–150 nM per AP) of bitufted interneurons by a factor of 2–4.

A potential caveat is deserved to discuss here. Large $[fura\text{-}2]_i$ will compete with the endogenous buffers and decrease $[Ca^{2+}]_i$ transient amplitudes. Could gradients in $[fura\text{-}2]_i$ have skewed spatial profile of Ca^{2+} transients? In addition to the effect of $[fura\text{-}2]_i$ on $[Ca^{2+}]_i$ transient amplitudes, large $[fura\text{-}2]_i$ can lengthen the decay (Fig. 3C); this make dye gradient easy to detect here (Svoboda et al., 1999). Because long decay times were not observed in the proximal dendrites (<20 μm, Fig. 3D), possible gradients in $[fura\text{-}2]_i$ might be low in this study and therefore compensation was not made.

Functional relevance

Somatostatin-containing interneurons are one of the most prevalent subpopulation of GABAergic interneurons in the stratum oriens of the CA1 region. Most of these neurons (the so-called O-LM cells) project massively to the stratum lacunosum-moleculare on the distal dendritic trees of pyramidal cells, whereas one third of the somatostatin containing interneurons co-expressing calbindin project to the medial septum (Tóth and Freund, 1992). In epileptic animals, 46% of somatostatin-containing interneurons in the stratum oriens/alveus are selectively degenerated (Cossart et al., 2001). Interestingly, many of the surviving somatostatin interneurons are calbindin-positive (Cossart et al., 2001). These observations strongly suggest a specific loss of O-LM cells, which lack the fast Ca^{2+}-buffer protein calbindin, in epileptic animals. Although the exact mechanism of this cell loss is unknown, some evidence suggests that selective vulnerability of O-LM cells may be due to Ca^{2+}-mediated toxicity (Woodhall et al., 1999; Gee et al., 2001). Interestingly, the expression of mobile Ca^{2+}-binding protein calbindin seems to confer some measure of neuroprotection in those surviving calbindin-positive somatostatin interneurons (Cossart et al., 2001). In line with the hypothesis, efficient Ca^{2+} buffering in fast-spiking basket cells may also account for the relative resistance of basket cells to epileptic seizures.

O-LM cells show low endogenous Ca^{2+} buffer capacities with large $[Ca^{2+}]_i$ elevations. Our results may add additional weight to the view that cytosolic Ca^{2+} overload is relevant to selective vulnerability of O-LM cells. Nevertheless, the causal link between the low κ_S and the selective vulnerability of O-LM cells to excitatotoxicity remain to be tested in the future study.

Dendritic Ca^{2+} dynamics and implications for synaptic plasticity

Ca^{2+} dynamics in neurons shaped by endogenous Ca^{2+} buffers may be important for the function of both input and output synapses (Schmidt et al., 2003a,b; Hefft and Jonas, 2005; Müller et al., 2007; Bucurenciu et al., 2008; Topolnik et al., 2009). Spike timing-dependent plasticity (STDP) is associated with the coincidence occurrence of presynaptic inputs and bAPs from postsynaptic target cells (Markram et al., 1997; Dan and Poo, 2004). The relative order of pre- and postsynaptic spikes within a short period can result in nonlinear summation of postsynaptic $[Ca^{2+}]_i$ in dendrites or spines. Large elevation of $[Ca^{2+}]_i$ can support long-term potentiation (LTP) induction, whereas moderate and prolonged $[Ca^{2+}]_i$ rise may underlie long-term depression (LTD) (Karmarkar and Buonomano, 2002; Malenka and Bear, 2004; Caporale and Dan, 2008). Thus, the Ca^{2+} dynamics is thought to be a key determinant for the temporal window of STDP induction. Recent studies showed that LTP can be readily induced and expressed in O-LM

cells and other inhibitory interneurons of the hippocampus (Kullmann and Lamsa, 2007; Oren et al., 2009). Intriguingly, both Hebbian and anti-Hebbian forms of LTP occur in O-LM cells (Kullmann and Lamsa, 2007; Topolnik et al., 2009): Hebbian LTP depends on activation of metabotropic GluRs, whereas anti-Hebbian one is through ionotropic GluR2-lacking α-amino-3-hydroxy-5-methyl-4-isoxazolepropionic acid receptor (AMPAR) activation. Activation of these two receptors causes intracellular Ca^{2+} elevation and leads to LTP. Therefore, understanding the details of Ca^{2+} dynamics, such as Ca^{2+} load and endogenous Ca^{2+}-binding ratios will provide information about the shape of global and local Ca^{2+} transient during synaptic transmission and backpropagating APs. Our results reveal that single APs effectively induce large Ca^{2+} transients over dendrites of O-LM cells and thus suggest that burst firing of O-LM cells preceding excitatory postsynaptic potentials (EPSPs) (opening of Ca^{2+}-permeable AMPARs) might lead to summation of large Ca^{2+} transients and might be more efficient for LTP induction.

Acknowledgments—We thank Drs. M.-M. Poo, M. Martina, T.C. Hwang and C.P. Hung for critically reading the manuscript and Dr. M. Martina for advice. This work was mainly supported by Ministry of Education, Taiwan (Aim for the Top University Plan), National Health Research Institutes (Grant NHRI-EX97-9720NC) and Taiwan National Science Council (Grant NSC97-2321-B-010-005).

REFERENCES

Aponte Y, Bischofberger J, Jonas P (2008) Efficient Ca^{2+} buffering in fast-spiking basket cells of rat hippocampus. J Physiol 586(8): 2061–2075.

Aponte Y, Lien CC, Reisinger E, Jonas P (2006) Hyperpolarization-activated cation channels in fast-spiking interneurons of rat hippocampus. J Physiol 574(1):229–243.

Bucurenciu I, Kulik A, Schwaller B, Frotscher M, Jonas P (2008) Nanodomain coupling between Ca^{2+} channels and Ca^{2+} sensors promotes fast and efficient transmitter release at a cortical GABAergic synapse. Neuron 57:536–545.

Caporale N, Dan Y (2008) Spike timing-dependent plasticity: a Hebbian learning rule. Annu Rev Neurosci 31:25–46.

Cobb SR, Buhl EH, Halasy K, Paulsen O, Somogyi P (1995) Synchronization of neuronal activity in hippocampus by individual GABAergic interneurons. Nature 378:75–78.

Cossart R, Dinocourt C, Hirsch JC, Merchan-Perez A, De Felipe J, Ben-Ari Y, Esclapez M, Bernard C (2001) Dendritic but not somatic GABAergic inhibition is decreased in experimental epilepsy. Nat Neurosci 4:52–62.

Csicsvari J, Hirase H, Czurkó A, Mamiya A, Buzsáki G (1999) Oscillatory coupling of hippocampal pyramidal cells and interneurons in the behaving rat. J Neurosci 19:274–287.

Dan Y, Poo MM (2004) Spike timing-dependent plasticity of neural circuits. Neuron 44:23–30.

Freund TF, Buzsáki G (1996) Interneurons of the hippocampus. Hippocampus 6:347–470.

Gee CE, Woodhall G, Lacaille JC (2001) Synaptically activated calcium responses in dendrites of hippocampal oriens-alveus interneurons. J Neurophysiol 85:1603–1613.

Gloveli T, Dugladze T, Saha S, Monyer H, Heinemann U, Traub RD, Whittington MA, Buhl EH (2005) Differential involvement of oriens/pyramidale interneurones in hippocampal network oscillations *in vitro*. J Physiol 562(1):131–147.

Goldberg JH, Lacefield CO, Yuste R (2004) Global dendritic calcium spikes in mouse layer 5 low threshold spiking interneurones: implications for control of pyramidal cell bursting. J Physiol 558(2): 465–478.

Goldberg JH, Tamas G, Yuste R (2003) Ca^{2+} imaging of mouse neocortical interneurone dendrites: Ia-type K^{+} channels control action potential backpropagation. J Physiol 551(1):49–65.

Goldberg JH, Yuste R (2005) Space matters: local and global dendritic Ca^{2+} compartmentalization in cortical interneurons. Trends Neurosci 28:158–167.

Grynkiewicz G, Poenie M, Tsien RY (1985) A new generation of Ca^{2+} indicators with greatly improved fluorescence properties. J Biol Chem 260:3440–3450.

Hartmann J, Konnerth A (2005) Determinants of postsynaptic Ca^{2+} signaling in Purkinje neurons. Cell Calcium 37:459–466.

Hefft S, Jonas P (2005) Asynchronous GABA release generates long-lasting inhibition at a hippocamapal interneuron-principal neuron synapse. Nat Neurosci 8:1319–1328.

Helmchen F, Borst JG, Sakmann B (1997) Calcium dynamics associated with a single action potential in a CNS presynaptic terminal. Biophys J 72:1458–1471.

Helmchen F, Imoto K, Sakmann B (1996) Ca^{2+} buffering and action potential-evoked Ca^{2+} signaling in dendrites of pyramidal neurons. Biophys J 70:1069–1081.

Helmchen F, Tank DW (2005) A single-compartment model of calcium dynamics in nerve terminals and dendrites. In: Imaging in neuroscience and development (Yuste R, Konnerth A, eds), pp 265–275. Cold Spring Harbor, NY: CSHL Publishing.

Jackson MB, Redman SJ (2003) Calcium dynamics, buffering, and buffer saturation in the boutons of dentate granule-cell axons in the hilus. J Neurosci 23:1612–1621.

Jonas P, Bischofberger J, Fricker D, Miles R (2004) Interneuron diversity series: fast in, fast out—temporal and spatial signal processing in hippocampal inerneurons. Trends Neurosci 27:30–40.

Kaiser KM, Zilberter Y, Sakmann B (2001) Back-propagating action potentials mediate calcium signalling in dendrites of bitufted interneurons in layer 2/3 of rat somatosensory cortex. J Physiol 535(1):17–31.

Kampa BM, Stuart GJ (2006) Calcium spikes in basal dendrites of layer 5 pyramidal neurons during action potential bursts. J Neurosci 26:7424–7432.

Kao JP, Tsien RY (1988) Ca^{2+} binding kinetics of fura-2 and azo-1 from temperature-jump relaxation measurements. Biophys J 53: 635–639.

Karmarkar UR, Buonomano DV (2002) A model of spike-timing dependent plasticity: one or two coincidence detectors? J Neurophysiol 88:507–513.

Klausberger T, Magill PJ, Márton LF, Roberts JD, Cobden PM, Buzsáki G, Somogyi P (2003) Brain-state- and cell-type-specific firing of hippocampal interneurons *in vivo*. Nature 421:844–848.

Klausberger T, Somogyi P (2008) Neuronal diversity and temporal dynamics: the unity of hippocampal circuit operations. Science 321:53–57.

Koh DS, Geiger JR, Jonas P, Sakmann B (1995) Ca^{2+}-permeable AMPA and NMDA receptor channels in basket cells of rat hippocampal dentate gyrus. J Physiol 485(2):383–402.

Kraushaar U, Jonas P (2000) Efficacy and stability of quantal GABA release at a hippocampal interneuron-principal neuron synapse. J Neurosci 20:5594–5607.

Kullmann DM, Lamsa KP (2007) Long-term synaptic plasticity in hippocampal interneurons. Nat Rev Neurosci 8:687–699.

Lawrence JJ, Statland JM, Grinspan ZM, McBain CJ (2006) Cell type-specific dependence of muscarinic signalling in mouse hippocampal stratum oriens interneurones. J Physiol 570(3):595–610.

Lee SH, Rosenmund C, Schwaller B, Neher E (2000) Differences in Ca^{2+} buffering properties between excitatory and inhibitory hippocampal neurons from the rat. J Physiol 525(2):405–418.

Lien CC, Jonas P (2003) Kv3 potassium conductance is necessary and kinetically optimized for high-frequency action potential generation in hippocampal interneurons. J Neurosci 23:2058–2068.

Lien CC, Martina M, Schultz JH, Ehmke H, Jonas P (2002) Gating, modulation and subunit composition of voltage-gated K^+ channels in dendritic inhibitory interneurones of rat hippocampus. J Physiol 538(2):405–419.

Lien CC, Mu Y, Vargas-Caballero M, Poo MM (2006) Visual stimuli-induced LTD of GABAergic synapses mediated by presynaptic NMDA receptors. Nat Neurosci 9:372–380.

Maccaferri G (2005) Stratum oriens horizontal interneurone diversity and hippocampal network dynamics. J Physiol 562(1):73–80.

Maccaferri G, Roberts JD, Szucs P, Cottingham CA, Somogyi P (2000) Cell surface domain specific postsynaptic currents evoked by identified GABAergic neurones in rat hippocampus *in vitro*. J Physiol 524(1):91–116.

Maglóczky Z, Freund TF (2005) Impaired and repaired inhibitory circuits in the epileptic human hippocampus. Trends Neurosci 28: 334–340.

Malenka RC, Bear MF (2004) LTP and LTD: an embarrassment of riches. Neuron 44:5–21.

Maravall M, Mainen ZF, Sabatini BL, Svoboda K (2000) Estimating intracellular calcium concentrations and buffering without wavelength ratioing. Biophys J 78:2655–2667.

Markram H, Lübke J, Frotscher M, Sakmann B (1997) Regulation of synaptic efficacy by coincidence of postsynaptic APs and EPSPs. Science 275:213–215.

Martina M, Schultz JH, Ehmke H, Monyer H, Jonas P (1998) Functional and molecular differences between voltage-gated K^+ channels of fast-spiking interneurons and pyramidal neurons of rat hippocampus. J Neurosci 18:8111–8125.

Martina M, Vida I, Jonas P (2000) Distal initiation and active propagation of action potentials in interneuron dendrites. Science 287: 295–300.

McBain CJ, Fisahn A (2001) Interneurons unbound. Nat Rev Neurosci 2:11–23.

Miles R, Tóth K, Gulyás AI, Hájos N, Freund TF (1996) Differences between somatic and dendritic inhibition in the hippocampus. Neuron 16:815–823.

Morin F, Beaulieub C, Lacaille JC (1998) Selective loss of GABA neurons in area CA1 of the rat hippocampus after intraventricular kainite. Epilepsy Res 32:363–369.

Müller M, Felmy F, Schwaller B, Schneggenburger R (2007) Parvalbumin is a mobile presynaptic Ca^{2+} buffer in the calyx of held that accelerates the decay of Ca^{2+} and short-term facilitation. J Neurosci 27:2261–2271.

Neher E (2008) Details of Ca^{2+} dynamics matter. J Phyisol 586(8): 2031.

Neher E, Augustine GJ (1992) Calcium gradients and buffers in bovine chromaffin cells. J Physiol 450:273–301.

Oren I, Nissen W, Kullmann DM, Somogyi P, Lamsa KP (2009) Role of ionotropic glutamate receptors in long-term potentiation in rat hippocampal CA1 oriens-lacunosum moleculare interneurons. J Neurosci 29:939–950.

Pottorf WJ, Duckles SP, Buchholz JN (2000) Mechanisms of calcium buffering in adrenergic neurones and effects of ageing: testing the limits of homeostasis. J Auton Pharmacol 20:63–75.

Pouille F, Scanziani M (2004) Routing of spike series by dynamic circuits in the hippocampus. Nature 429:717–723.

Rozsa B, Zelles T, Vizi ES, Lendvai B (2004) Distance-dependent scaling of calcium transients evoked by backpropagating spikes and synaptic activity in dendrites of hippocampal interneurons. J Neurosci 24:661–670.

Sabatini BL, Oertner TG, Svoboda K (2002) The life cycle of Ca^{2+} ions in dendritic spines. Neuron 33:439–452.

Scheuss V, Yasuda R, Sobczyk A, Svoboda K (2006) Nonlinear $[Ca^{2+}]$ signaling in dendrites and spines caused by activity-dependent depression of Ca^{2+} extrusion. J Neurosci 26:8183–8194.

Schmidt H, Brown EB, Schwaller B, Eilers J (2003a) Diffusional mobility of parvalbumin in spiny dendrites of cerebellar Purkinje neurons quantified by fluorescence recovery after photobleaching. Biophys J 84:2599–2608.

Schmidt H, Stiefel KM, Racay P, Schwaller B, Eilers J (2003b) Mutational analysis of dendritic Ca^{2+} kinetics in rodent Purkinje cells: role of parvalbumin and calbindin D_{28k}. J Physiol 551(1):13–32.

Sloviter RS, Zappone CA, Harvey BD, Bumanglag AV, Bender RA, Frotscher M (2003) "Dormant basket cell" hypothesis revisited: relative vulnerabilities of dentate gyrus mossy cells and inhibitory interneurons after hippocampal status epilepticus in the rat. J Comp Neurol 459:44–76.

Stocca G, Schmidt-Hieber C, Bischofberger J (2008) Differential dendritic Ca^{2+} signaling in young and mature hippocampal granule cells. J Physiol 586(16):3795–3811.

Svoboda K, Helmchen F, Denk W, Tank DW (1999) Spread of dendritic excitation in layer 2/3 pyramidal neurons in rat barrel cortex *in vivo*. Nat Neurosci 2:65–73.

Topolnik L, Chamberland S, Pelletier JG, Ran I, Lacaille JC (2009) Activity-dependent compartmentalized regulation of dendritic Ca^{2+} signaling in hippocampal interneurons. J Neurosci 29:4658–4663.

Tóth K, Freund TF (1992) Calbindin D28k-containing nonpyramidal cells in the rat hippocampus: their immunoreactivity for GABA and projection to the medial septum. Neuroscience 49:793–805.

Woodhall G, Gee CE, Robitaille R, Lacaille JC (1999) Membrane potential and intracellular Ca^{2+} oscillations activated by mGluRs in hippocampal stratum oriens/alveus interneurons. J Neurophysiol 81:371–382.

Yasuda R, Nimchinsky EA, Scheuss V, Pologruto TA, Oertner TG, Sabatini BL, Svoboda K (2004) Imaging calcium concentration dynamics in small neuronal compartments. Sci STKE 219: pl5.

Zhao M, Hollingworth S, Baylor SM (1996) Properties of tri- and tetracarboxylate Ca^{2+} indicators in frog skeletal muscle fibers. Biophys J 70:896–916.

Zheng JQ, Poo MM (2007) Calcium signaling in neuronal motility. Annu Rev Cell Dev Biol 23:375–404.

APPENDIX

Supplementary data

Supplementary data associated with this article can be found, in the online version, at doi:10.1016/j.neuroscience.2009.09.052.

(Accepted 19 September 2009)
(Available online 25 September 2009)